J Mol Model (2014) 20:2451
DOI 10.1007/s00894-014-2451-x

ORIGINAL PAPER

Novel theoretically designed HIV-1 non-nucleoside reverse transcriptase inhibitors derived from nevirapine

Jinfeng Liu · Xiao He · John Z. H. Zhang

Received: 26 December 2013 / Accepted: 1 September 2014 / Published online: 20 September 2014

Abstract A common problem with non-nucleoside reverse transcriptase inhibitors (NNRTIs) of HIV-1 is the emergence of mutations in the HIV-1 RT, in particular Lys103→Asn (K103N) and Tyr181→Cys (Y181C), which lead to resistance to this entire class of inhibitors. In this study, we theoretically designed two new non-nucleoside HIV-1 RT inhibitors, Mnev-1 and Mnev-2, derived from nevirapine, in order to reduce the resistance caused by those HIV-1 RT mutations. The binding modes of Mnev-1 and Mnev-2 with the wild-type HIV-1 RT and its mutants (K103N and Y181C) were suggested by molecular docking followed by 20-ns molecular dynamics (MD) simulations in explicit water of those binding complexes (HIV-1 RTs with the new inhibitors). A molecular mechanics/generalized Born surface area (MM/GBSA) calculation was carried out for multiple snapshots extracted from the MD trajectory to estimate the binding free energy. The results of the calculations show that each of the new inhibitors forms a stable hydrogen bond with His235 during the MD simulations, leading to tighter binding of the new inhibitors with their targets. In addition, the repulsive interaction with Cys181 in the Y181C–nevirapine complex is not present in the novel inhibitors. The binding affinities predicted using the MM/GBSA calculations indicate that the new inhibitors could be effective at bypassing the drug resistance of these HIV-1 RT mutants.

Keywords HIV-1 reverse transcriptase · Non-nucleoside reverse transcriptase inhibitor · Nevirapine · Mutation · Drug resistance · Molecular docking · Molecular dynamics simulation · MM/GBSA · Hydrogen bonding

Introduction

An essential part of the life cycle of HIV-1 is the transcription of single-stranded viral genomic RNA into double-stranded DNA by the enzyme reverse transcriptase (RT) [1]. RT is an excellent target for drug design because it is essential for HIV replication but not required for normal cell replication. The compounds that inhibit the DNA polymerase activity of RT can be divided into two broad classes: (1) the nucleoside reverse transcriptase inhibitor (NRTI), which inhibits viral replication by acting as the chain terminator of DNA synthesis [1], and (2) the non-nucleoside reverse transcriptase inhibitor (NNRTI), which binds to a site in the RT "palm" sub-domain adjacent to but distinct from the polymerase active site [2–6].

NNRTIs are key components of highly active antiretroviral therapy for the treatment of HIV-1. Many NNRTIs, which are highly specific and less toxic than NRTIs, have been developed and are prescribed clinically [7, 8]. However, a common problem with NNRTIs is the emergence of mutations in the HIV-1 RT, in particular Lys103→Asn (K103N) and Tyr181→Cys (Y181C), which lead to resistance to this entire class of inhibitors [9]. Nevirapine is a first-generation FDA-approved NNRTI, but its therapeutic effectiveness is limited by the relatively rapid emergence of drug-resistant HIV-1 mutants [10, 11]. Thus, the discovery of new and more potent inhibitors has become increasingly important in

Electronic supplementary material The online version of this article (doi:10.1007/s00894-014-2451-x) contains supplementary material, which is available to authorized users.

J. Liu · X. He (✉) · J. Z. H. Zhang
State Key Laboratory of Precision Spectroscopy and Department of Physics, Institute of Theoretical and Computational Science, East China Normal University, Shanghai 200062, China
e-mail: xiaohe@phy.ecnu.edu.cn

X. He · J. Z. H. Zhang
NYU-ECNU Center for Computational Chemistry at NYU Shanghai, Shanghai 200062, China

light of the emergence of HIV strains that are resistant to current drugs [12].

The rapidity of the selection of drug-resistant HIV in patients is such that mutations of amino acid residues in the binding pocket of RT reduce the effect of the drug significantly and make first-generation NNRTIs such as nevirapine unusable in monotherapy [10]. An important mutation (lysine to asparagine) for residue 103 of the RT p66 subunit [13, 14]. The reduction in binding affinity to nevirapine caused by this mutation is 40-fold or more [15]. Another important mutation in RT occurs at Tyr181, which gives rise to high-level resistance [11, 16]. This mutation has been frequently reported in studies of resistance to many other NNRTIs, and the Tyr is almost always changed to Cys [17]. Nevirapine shows a 113-fold drop in binding affinity to Y181C compared to the wild-type RT [15, 18].

Several studies have attempted to find better NNRTIs that are active against drug-resistant mutants [19–23]. Parrish et al. evaluated the efficacy of a series of nevirapine-based analogs containing the phosphonate functionality against HIV-1 RT, and found that the compounds with a phosphonate group had excellent antiviral activities against the wild-type HIV-1 RT and the mutant Y181C [21]. Rizzo et al. also explored the effects of twenty nevirapine analogs on HIV-1 RT and revealed their structures using Monte Carlo simulations. They concluded that the loss of hydrogen bonds with nevirapine upon binding was a major cause of the drug resistance exhibited by HIV-1 RT mutants [22–24].

In a previous study, to gain a comprehensive understanding of the RT–drug binding interaction and the origin of the effects of mutating RT, we performed fully quantum-mechanical calculations at the HF/3-21G level to investigate the interactions associated with the binding of nevirapine to HIV-1 RT and its mutants K103N and Y181C [2]. The full ab initio computation of the biomacromolecule was made possible by applying the molecular fractionation with conjugate caps (MFCC) approach [25–27]. The MFCC approach developed for the full quantum chemical computation of protein interaction energies is especially convenient for the protein–ligand binding interaction [25], and has been successfully applied to calculate the interaction energies of several protein–ligand systems [28–36]. In our previous study, we found that nevirapine binds to HIV-1 RT through several weak hydrogen bonds and that the dominant binding is to His235, Pro236, and Lys101. A fundamental reason for the significant loss of binding affinity of the first-generation drug nevirapine to mutants of HIV-1 RT is that there are no strong hydrogen bonds between the drug and the enzyme. Thus, a change in the conformation of the RT–drug complex due to mutation can easily weaken the weak binding interactions. It is thus highly desirable to build stable hydrogen bonds with the conservative residues of the enzyme by modifying nevirapine. Furthermore, for the mutant Y181C, there is a further loss of nevirapine binding affinity to the enzyme due to strong repulsion between a carbon atom of nevirapine and the sulfur atom in the side chain of the mutated Cys181 [2]. Taking all of these factors into consideration, we propose two new nevirapine-based inhibitors to improve drug efficacy against HIV-1 RT and its mutants.

Many computational methods have been utilized for predicting protein–ligand binding affinities. Among the approximate methods employed, the molecular mechanics Poisson Boltzmann or generalized Born surface area (MM-PB/GBSA) approach is attractive because it does not include any parameters that vary for different protein–ligand systems, and it involves a set of physically well-defined energy terms [37–39]. This approach is efficient, accurate, and less computationally demanding [4, 40]. Here, we apply a combination of molecular dynamics (MD) and MM/GBSA [37, 38, 41] techniques to analyze the interactions between the new inhibitors and HIV-1 RT, and the impact of mutations on the binding affinities of the new inhibitors. The GB parameters are usually chosen to match experimental solvation free energies [42, 43]. According to a previous study by Hou and co-workers, MM/GBSA shows better performance than MM/PBSA in ranking the binding affinities for systems without metals [44]. As the main purpose of this study is to predict the relative binding affinities due to mutations for the new inhibitors, MM/GBSA thus appears to be more appropriate than MM/PBSA for this study. In addition, the MM/GBSA method has been successfully applied to estimate the binding free energies of protein–ligand systems, including various inhibitors with HIV-1 RTs [9, 45].

In this study, we designed two new NNRTIs derived from nevirapine to reduce the drug resistance of HIV-1 RT mutants. MM/GBSA calculations were carried out to predict the binding affinities of the newly proposed inhibitors for the wild-type HIV-1 RT and the mutants K103N and Y181C. The results were compared with those obtained for nevirapine. The effectiveness of the new inhibitors in bypassing the drug resistance of the HIV-1 RT mutants is discussed below in detail.

Computational approach

Constructing the new inhibitors

The crystal structures of HIV-1 RT and its two mutants were retrieved from the Protein Data Bank. The PDB ids for the wild type, K103N, and Y181C are 1VRT, 1FKP, and 1JLB, respectively. Nevirapine (Fig. 1a) was extracted from the corresponding structure. Based on the structural analysis, we modified nevirapine by adding a hydroxyl group to the C13 atom for constructing potential hydrogen bonds to His235 and Tyr318 of HIV-1 RT. In addition, we exchanged the positions

of C4 and N2 to avoid the repulsion caused by Cys181 in the Y181C mutant [2]. This exchange was performed because the atomic radius of the nitrogen atom is smaller than that of carbon, and an S–H···N2 hydrogen bond may form between the mutated Cys181 and the modified ligand. We also exchanged the positions of two groups (N3–H1 and C10=O1) to avoid the possible formation of an internal hydrogen bond between C10=O1 and the added hydroxyl group, which would not be favorable for constructing stable hydrogen bonds to His235 and Tyr318. We named the new inhibitor "Mnev-1," as shown in Fig. 1b. Since we added a polar group to nevirapine, which could increase the solvation energy as compared to nevirapine, we also modified the structure of Mnev-1 by replacing N4 with a carbon atom (C16) to balance the number of polar groups. The new molecule was named "Mnev-2" (Fig. 1c).

Molecular docking

The Autodock program [46] (version 4.2) was employed to generate an ensemble of docked conformations for the new inhibitors bound to the wild-type HIV-1 RT and its mutants. We used a genetic algorithm (GA) to perform conformational searches. To explore the conformational space of the new inhibitor as completely as possible, we performed 100 individual GA runs to generate 100 docked conformations for each inhibitor. The size of the docking box was 60 Å×60 Å×60 Å, and this was centered at the center of mass of the experimentally observed position of nevirapine. This box, with a grid spacing of 0.375 Å, was large enough to enclose the binding pocket. The protein structure was kept fixed during molecular docking. To validate the reliability of Autodock, we also docked nevirapine to the target using the same procedure, and compared the docked conformation with its crystal structure. In this work, the conformation that has the most favorable docking free energy was chosen for further study.

Preparation of the protein–ligand complexes

Hydrogen atoms were added to the wild-type HIV-1 RT and its mutants using the Leap module in Amber11 [47]. The amine groups were fully protonated (Lys and Arg residues and N-terminus), and the carboxylic groups were deprotonated (Asp and Glu residues and C-terminus). All His residues were left neutral and protonated at the ND1 or NE2 position based on the local electrostatic environment. Partial charges of the protein were assigned with the Amber ff99SB force field [48]. Hydrogen atoms were added to nevirapine and the newly proposed inhibitors (Mnev-1 and Mnev-2) using Discovery Studio. The geometry of the ligand was optimized at the HF/6-31G* level. The force field parameters of the ligand were subsequently obtained using the ANTECHAMBER module [49] based on the generalized Amber force field (GAFF) [50]

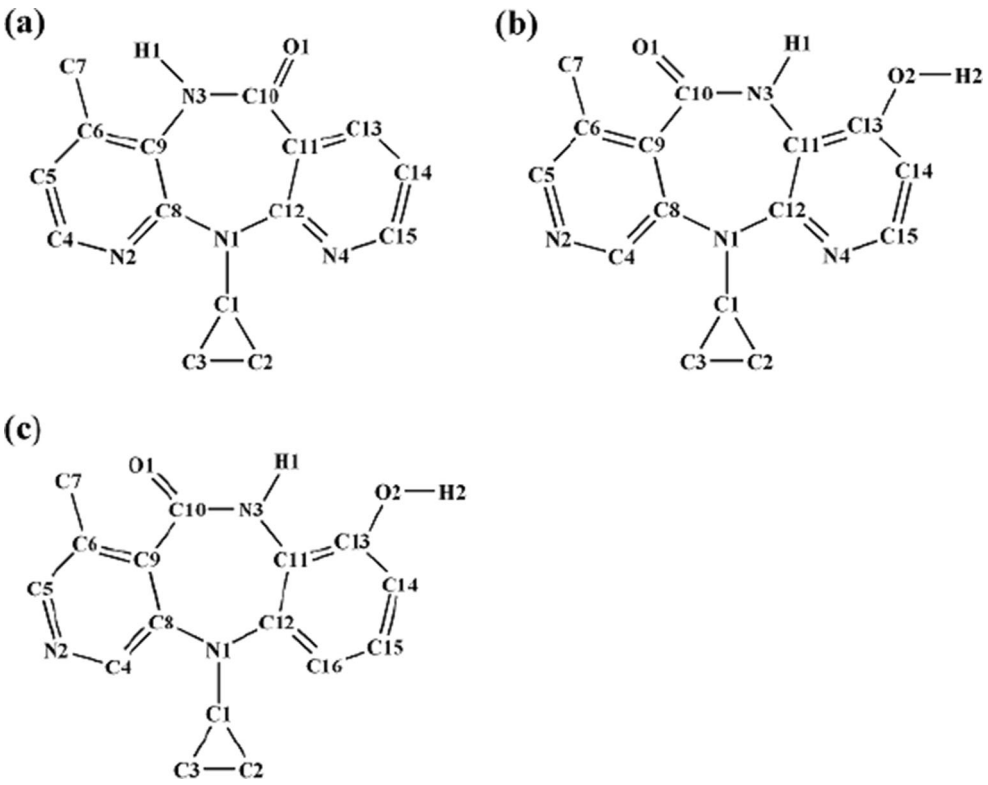

Fig. 1 **a**–**c** Molecular structures of the inhibitors **a** nevirapine, **b** Mnev-1, and **c** Mnev-2

with the HF/6-31G* RESP charges [51, 52]. All ab initio calculations were carried out using the Gaussian 09 program [53].

MD simulation

In the MD simulations, each complex was immersed in a periodic rectangular box of TIP3P water molecules. The distance from the surface of the box to the closest atom of the solute was set to 10 Å. Counterions were added to neutralize the system. The particle mesh Ewald (PME) method was employed to treat the long-range electrostatic interactions [54]. The simulations were conducted by first performing two minimization stages to optimize the initial structure. In the first stage, only the solvent molecules and hydrogen atoms of the protein–ligand complex were optimized by carrying out 5000 steps of a steepest descent algorithm followed by another 5000 steps of conjugate gradient minimization. In the second stage, the energy of the entire system was minimized until convergence was reached. After this two-stage minimization, the system was then gradually heated from 0 to 300 K in 100 ps (NVT ensemble), followed by a 20-ns NPT simulation at 300 K and 1 atm with a time step of 2 fs. The SHAKE algorithm was employed to restrain all bonds involving hydrogen atoms [55]. A 10-Å cutoff for van der Waals interactions was adopted. Langevin dynamics [56] was applied to regulate the temperature with a collision frequency of 2.0 ps^{-1}. The pressure was controlled by the isotropic position scaling protocol. All MD simulations were performed with the Amber11 program [47].

MM/GBSA and normal-mode calculations

In MM/GBSA calculations, the protein–ligand binding affinity is determined according to the following equation:

$$\Delta G_{\text{bind}} = G_{\text{complex}} - G_{\text{receptor}} - G_{\text{ligand}} \quad (1)$$

$$= \Delta E_{\text{MM}} + \Delta G_{\text{GB}} + \Delta G_{\text{nonpolar}} - T\Delta S, \quad (2)$$

where ΔE_{MM} is the gas-phase interaction energy between protein and ligand, including the electrostatics and van der Waals energies; ΔG_{GB} is the polar contribution to the solvation free energy, estimated from the solution of the general Born (GB) equation; $\Delta G_{\text{nonpolar}}$ is the nonpolar solvation free energy; and $T\Delta S$ is the change in conformational entropy upon ligand binding. To solve the GB equation, the value of the exterior dielectric constant is set to 80 and the solute dielectric constant is set to 1. The nonpolar solvation term is calculated from the solvent-accessible surface area (SASA) [57]: $\Delta G_{\text{nonpolar}} = \gamma \times \Delta\text{SASA}$, where $\gamma = 0.0072$ kcal/(mol $Å^2$). The entropic contribution to the binding free energy is calculated via normal-mode analysis [58]. To obtain the ensemble-averaged binding free energies, 50 snapshots were evenly extracted along the MD simulation after the systems were well equilibrated. The normal-mode calculation is extremely time-consuming for large systems, so only residues that can be within 15 Å of the inhibitor were used for the normal-mode calculation, and only the last 20 of the 50 selected snapshots were used to estimate the contribution of the entropy [4].

Results and discussion

Binding modes of Mnev-1 and Mnev-2 to HIV-1 RTs

Following structural inspection, we added a hydroxyl group to the C13 atom of nevirapine to construct potential hydrogen bonds with the His235 and Tyr318 of HIV-1 RT. We also exchanged the relative positions of C4 and N2 to avoid the repulsion caused by Cys181 in the Y181C mutant. Figures 2a and b show the two possible conformations if the two groups N3–H1 and C10=O1 are not exchanged. The relative electronic energies of these two conformations calculated at the B3LYP/6–311+G** level are shown in Table 1. It can be seen that the structure with the internal hydrogen bond is more stable (10.95 kcal/mol^{-1} lower than the other one). Hence, it would not be favorable to construct a hydrogen bond between the added hydroxyl group (O2–H2) and His235 or Tyr318. This may be consistent with the findings of an early experimental study [59], in which the hydroxyl group was substituted at the same place but the inhibition potency was not improved. Therefore, we further exchanged the positions of N3–H1 and C10=O1 and proposed the potential active inhibitor Mnev-1. We also compared the two possible conformations of Mnev-1, as shown in Fig. 2c and d. The relative conformational energies of those two conformations are also given in Table 1. The energy of conformation (d) is 0.49 kcal/mol^{-1} lower than that of conformation (c), so it should be more favorable for the hydroxyl group to be the hydrogen-bond donor to the residues in the target.

To validate the reliability of Autodock in predicting the binding modes for our new proposed ligands, we first docked nevirapine into the HIV-1 RT and compared the result with the experimentally observed binding mode. We found that Autodock successfully predicted the correct binding mode for nevirapine. The top-ranked conformation was remarkably close to the experimental structure and the root-mean-square deviation (RMSD) was only 0.68 Å. We therefore followed the same procedure to dock Mev-1 and Mnev-2 into the HIV-1 RT and its mutants using Autodock. The binding structures of

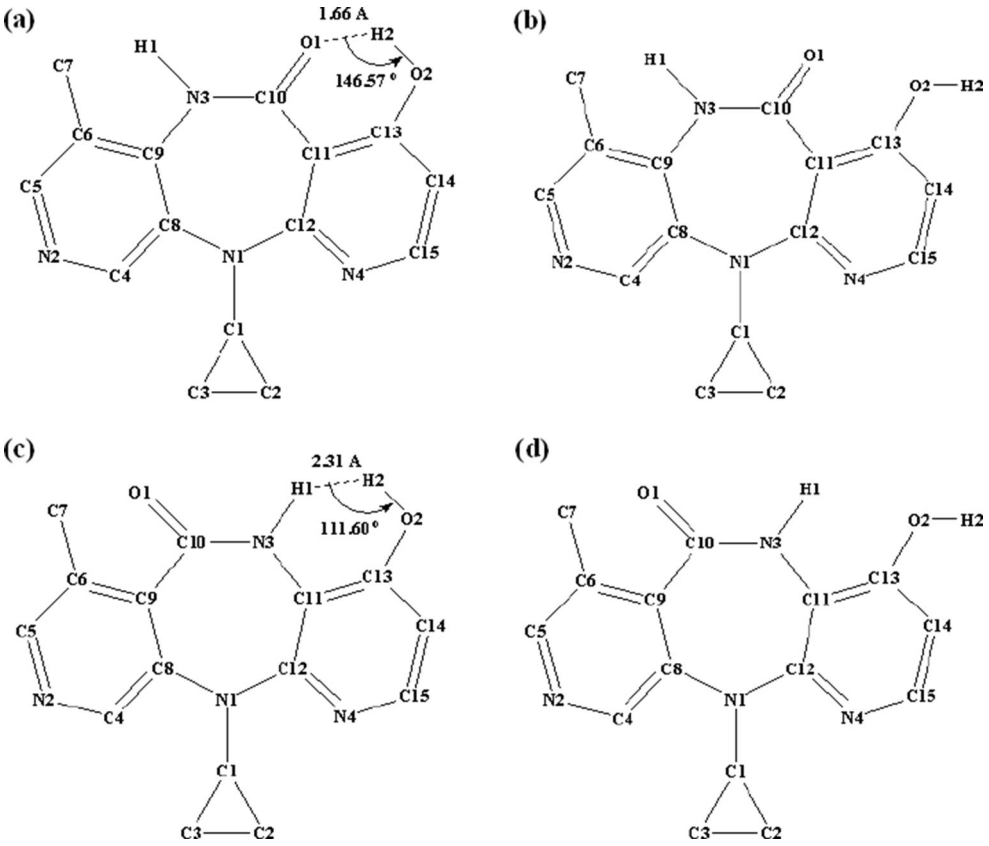

Fig. 2 Four conformers optimized at the B3LYP/6–311+G** level for the structure-based study

the new inhibitors are very close to nevirapine, as shown in Fig. 3. The binding mode of Mnev-1 with the wild-type HIV-1 RT is shown in Fig. 4. As expected, the added hydroxyl group in Mnev-1 forms two hydrogen bonds with His235 and Tyr318, respectively. According to our previous study [2], Cys181 in Y181C has a repulsive interaction with C4 in nevirapine. After we exchanged the positions of N2 and C4, that repulsive interaction diminished and the interaction even became slightly attractive since a new N2···H–S hydrogen bond formed, as shown in Fig. 5. The hydrogen bonds between Mnev-1 and RT mutants (K103N and Y181C), Mnev-2, and HIV-1 RTs are shown in Fig. S1 of the "Electronic supplementary material," ESM.

MD simulations of Mnev-1 and Mnev-2 with HIV-1 RTs

The RMSDs of the backbone atoms with respect to the initial docked structures during the MD simulation are plotted in Fig. 6. This figure clearly shows that, for all of the studied systems, the RMSD of the protein increases during the first 1 ns of the MD simulation. After that, the overall RMSD is stable and mostly fluctuates between 2.0 and 2.5 Å. All of the inhibitors are localized in the binding pocket since the RMSD of each inhibitor is only ~0.5 Å. This is not surprising because nevirapine has only two restricted rotatable bonds and each new inhibitor (Mnev-1 or Mnev-2) has only one more. All of these inhibitors are very rigid and their translational and rotational motions are slight in the binding pocket.

Both Mnev-1 and Mnev-2 could potentially form hydrogen bonds with His235 and Tyr318, as suggested by molecular docking. To verify the stability of the hydrogen bonds, we plotted the hydrogen-bond distances between the H2 atom in the hydroxyl group of each new inhibitor and the oxygen atom in the peptide bond of His235 or the oxygen atom in the side chain of Tyr318, as shown in Fig. 7. One can see from the figure that the distance between the H2 atom of the new inhibitor (Mnev-1 or Mnev-2) and the oxygen atom of His235 is around 1.80 Å. In contrast, the distance between

Table 1 Molecular electronic energies of conformers (a)–(d) in Fig. 2 calculated at the B3LYP/6-311+G** level

Conformer	Energy (au)	Relative energy (kcal/mol^{-1})	Conformer	Energy (au)	Relative energy (kcal/mol^{-1})
(a)	−949.726802	0.00	(c)	−949.708383	0.00
(b)	−949.709348	10.95	(d)	−949.709166	−0.49

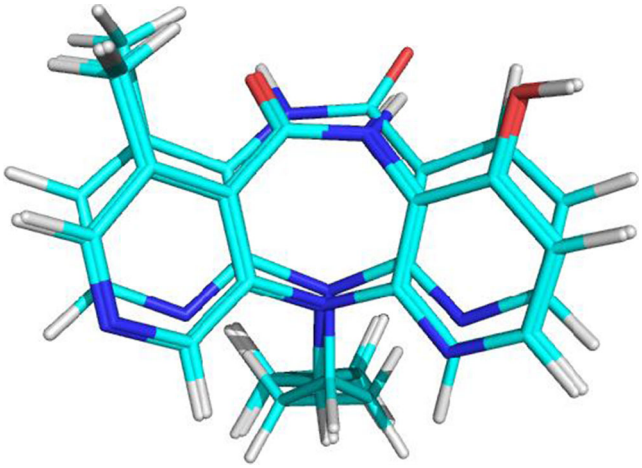

Fig. 3 Superimposed binding structures of nevirapine, Mnev-1, and Mnev-2 in the binding pocket of the wild-type HIV-1 RT

the H2 atom of the new inhibitor and the oxygen atom of Tyr318 is around 3.00 Å. The hydrogen bond between the new inhibitor and His235 is more favorable than that between the new inhibitor and Tyr318 in each system. Moreover, the hydrogen bond between each new inhibitor and His235 is stable not only for the wild-type HIV-1 RT but also for the mutants (K103N and Y181C) during MD simulation. The binding of each new inhibitor with the protein is enhanced by the strong hydrogen bond, which may help to reduce the drug resistance of the HIV-1 RT mutants.

Binding affinity prediction

We finally calculated the binding affinity of each new inhibitor with the wild-type HIV-1 RT, K103N, and Y181C,

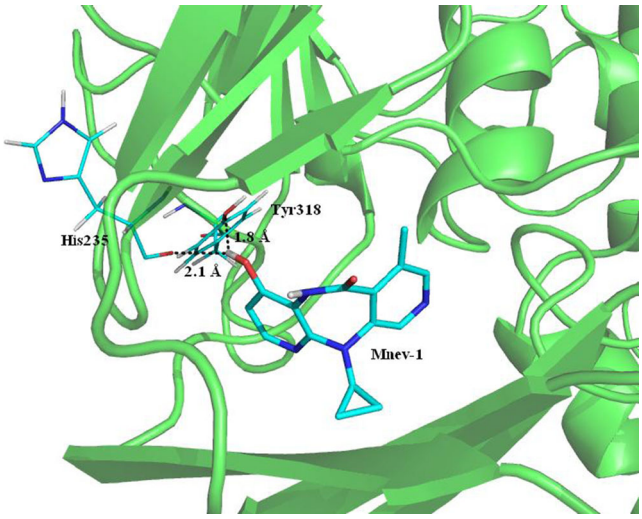

Fig. 4 Binding mode of Mnev-1 with wild-type HIV-1 RT, as suggested by Autodock. Mnev-1 is shown as *sticks* while His235 and Tyr318 are shown as *lines*. Potential hydrogen bonds between Mnev-1 and protein residues are shown as *dashed lines*

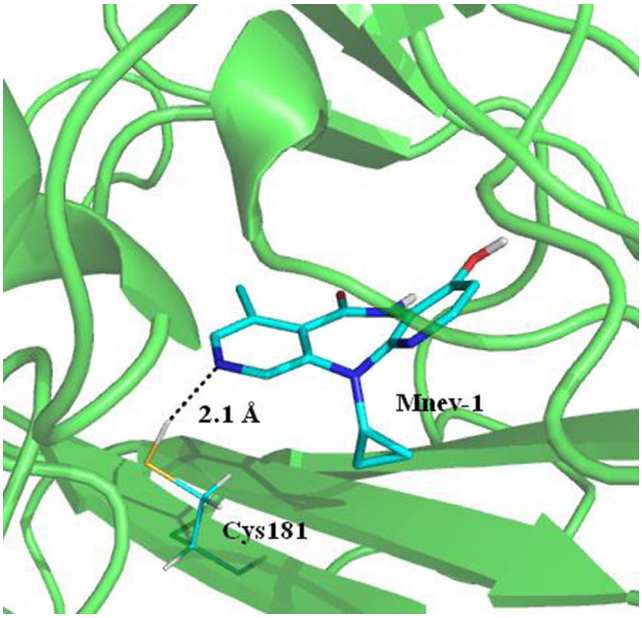

Fig. 5 Interaction between Mnev-1 and Cys181 in the mutant Y181C. Mnev-1 is shown as *sticks* while Cys181 is shown as *lines*. The potential hydrogen bond between Mnev-1 and Cys181 is shown as a *dashed line*

respectively. The binding free energies obtained from MM/GBSA calculations are shown in Table 2. To elucidate the binding mechanism, the binding energies were decomposed into contributions from the electrostatic interaction (ΔE_{ele}), van der Waals interaction (ΔE_{vdw}), the polar (ΔG_{pol}) and nonpolar (ΔG_{np}) solvation free energies, and the change of entropy ($T\Delta S$) upon binding.

Nevirapine Our calculations show that the total binding free energy for nevirapine with the wild-type HIV-1 RT is −14.75 kcal/mol^{-1}. However, it increases to −12.14 and −13.32 kcal/mol^{-1} for the mutants K103N and Y181C, respectively. Hence, the single mutations in K103N and Y181C reduce the binding affinity significantly, by approximately 2.61 and 1.43 kcal/mol^{-1}, respectively. A general feature is that the most prominent binding contributions originate from the van der Waals (VDW) interactions, which are fairly close to each other for three HIV-1 RTs (−43.15, −43.54, and −42.50 kcal/mol^{-1} for the wild-type HIV-1 RT, K103N, and Y181C, respectively). In addition, the nonpolar contributions to the solvation free energy are around −4.72 to−4.83 kcal/mol^{-1}. The ΔE_{ele}, ΔG_{pol}, and $T\Delta S$ values differ significantly due to the mutations. The attractive ΔE_{ele} term is canceled out by the unfavorable ΔG_{pol} energy. The sum of ΔE_{ele} and ΔG_{pol} is 15.07, 15.99, and 14.77 kcal/mol^{-1} for the wild type, K103N, and Y181C, respectively. For K103N, it becomes more unfavorable due to the mutation (15.99 kcal/mol^{-1} vs 15.07 kcal/mol^{-1}). However, for Y181C, it becomes slightly more favorable due to the mutation (14.77 kcal/mol^{-1} vs 15.07 kcal/mol^{-1}). Moreover, the loss of binding energy for the mutants is mostly attributed

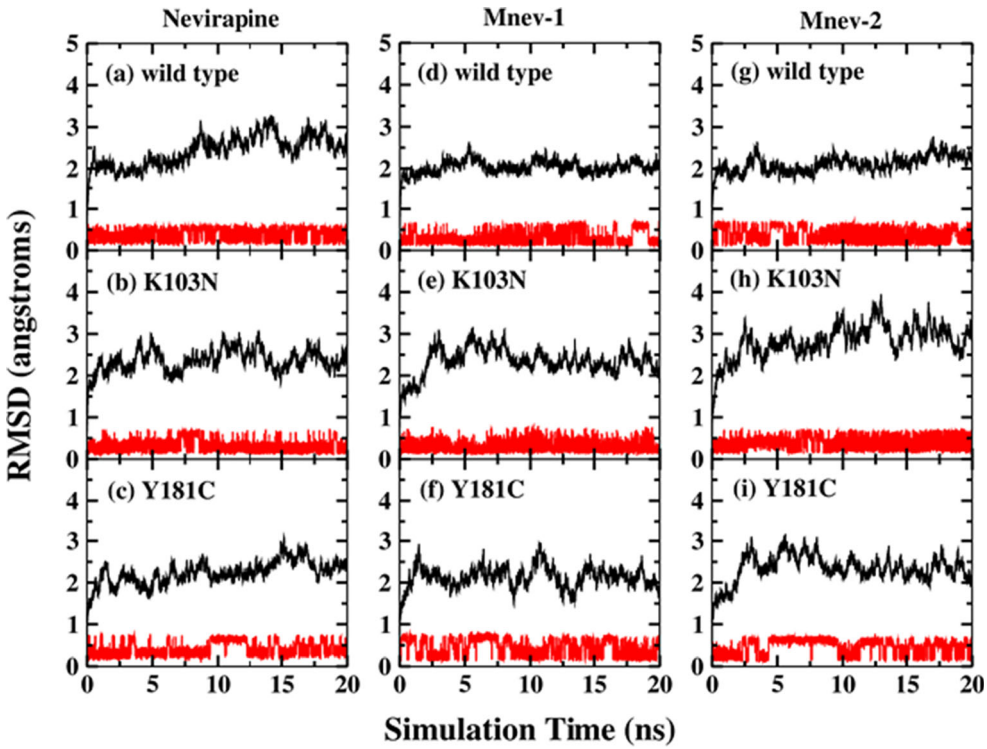

Fig. 6 RMSD of the backbone atoms of the protein (*black*) and ligand (*red*) during MD simulations

to changes in $T\Delta S$, which are −18.08, −20.14, and −19.24 kcal/mol^{-1}, respectively, for the wild type, K103N, and Y181C.

From the experiment of Sardana et al. [15], the binding free energy of nevirapine with Y181C is −6.34 kcal/mol^{-1}, which is higher than that (−6.96 kcal/mol^{-1}) of nevirapine bound to K103N by 0.62 kcal/mol^{-1}. In our previous ab initio study [2], we also found that for Y181C, a further loss of nevirapine binding affinity for the enzyme was caused by a strong

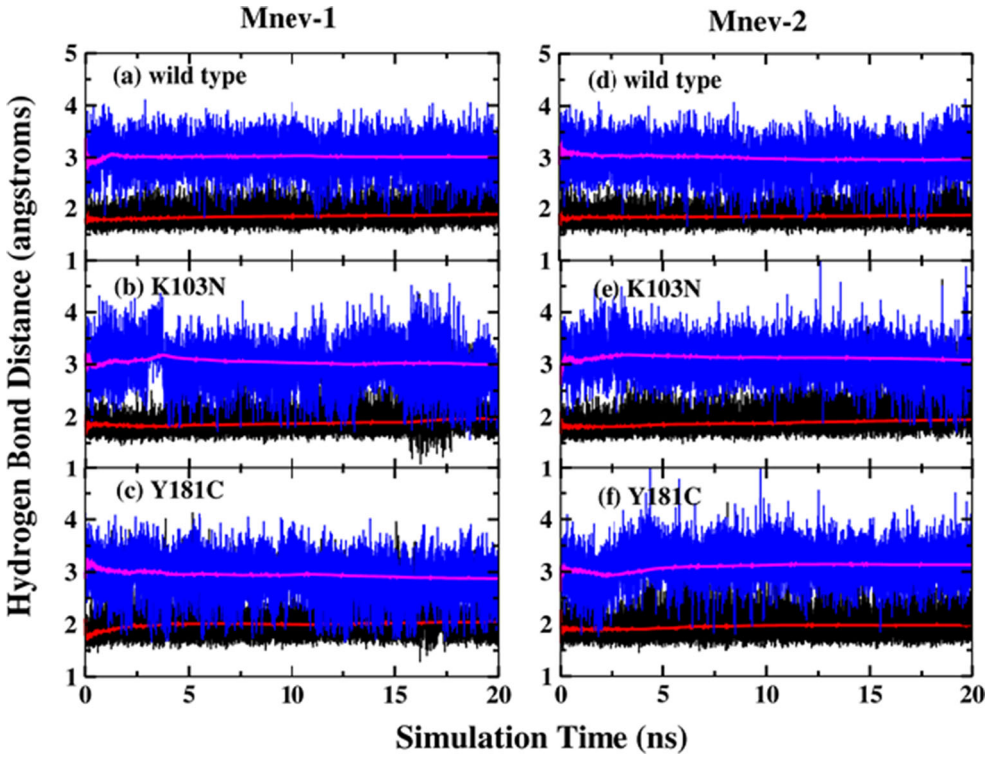

Fig. 7 Hydrogen-bond distances between the hydrogen of the hydroxyl group in Mnev-1 (or Mnev-2) and the acceptors of His235 (*black*) and Tyr318 (*blue*) in HIV-1 RTs, respectively, during MD simulations. The *pink and red lines* represent the time-averaged distances

Table 2 Free energy terms (in kcal/mol^{-1}) for the binding of inhibitors with the wild-type HIV-1 RT and its mutants K103N and Y181C, respectively, based on MM/GBSA calculations

Inhibitor	RT	ΔE_{ele}	ΔE_{vdw}	ΔG_{pol}	ΔG_{np}	$T\Delta S$	ΔG_{bind}	ΔG_{exp} [a]
Nevirapine	Wild type	−7.03	−43.15	22.10	−4.75	−18.08	−14.75	−9.15
	K103N	−3.78	−43.54	19.77	−4.72	−20.14	−12.14	−6.96
	Y181C[b]	−6.57	−42.50	21.34	−4.83	−19.24	−13.32	−6.34
	Y181C[c]	−6.33	−42.03	21.92	−4.75	−20.90	−10.29	
Mnev-1	Wild type	−10.27	−42.04	27.79	−4.95	−16.27	−13.20	
	K103N	−12.73	−44.49	30.60	−4.68	−15.73	−15.57	
	Y181C[b]	−12.09	−44.33	30.06	−4.90	−15.76	−15.50	
Mnev-2	Wild type	−6.75	−44.14	23.89	−4.96	−19.67	−12.29	
	K103N	−11.37	−44.33	27.31	−4.89	−18.51	−14.76	
	Y181C[b]	−8.85	−44.57	24.80	−4.83	−17.13	−16.32	

[a] From [61] and [15]

[b] The VDW parameters of sulfur were the same as the original ones in the Amber ff99SB force field. The VDW radius was 2.00 Å and ε was 0.25 for sulfur. The VDW parameters of sulfur were unchanged for interaction with the nitrogen atom (see Fig. 8b)

[c] The VDW parameters of sulfur were refitted (the VDW radius was 1.80 Å and ε was 0.20) for interaction with the carbon atom based on ab initio calculations (see Fig. 8a)

repulsion between the C4 carbon atom of nevirapine and the sulfur atom in the side chain of the mutated Cys181. However, our present results show that the calculated binding energy of nevirapine with Y181C is even lower than that of nevirapine bound to K103N by 1.18 kcal/mol^{-1}, which contradicts the experimental results and our previous ab initio calculations. To further investigate this, we computed the interaction energy between nevirapine and Cys181 at the M06L/6–311++G** level, and compared the result with that obtained from the Amber force field. The Ace and Nme residues were added on both sides of Cys181 to saturate the dangling bonds. The energy profile as a function of the distance between the C4 atom of nevirapine and the sulfur atom of the side chain of Cys181 is shown in Fig. 8a. As shown in the figure, the potential energy minimum computed by the Amber force field is deeper than that calculated by quantum mechanics (QM) (by about 1.08 kcal/mol^{-1}). Therefore, the interaction energy between nevirapine and Cys181 described by the Amber force field is too attractive. To align the empirical interaction energy profile more closely with the QM curve, we tuned the van der Waals (VDW) parameters of the sulfur atom of the CYS residue. The original VDW radius is 2.00 Å and ε is 0.25 for the sulfur atom in the Amber force field [60]. We set the VDW radius and ε of the sulfur atom to be 1.80 Å and 0.20, respectively. As shown in Fig. 8a, the new energy profile with the modified VDW parameters is closer to the QM curve, although the new energy minimum is still deeper by about 0.71 kcal/mol^{-1} than that of the QM curve. We applied the new VDW parameters of sulfur to perform an MD simulation and an MM/GBSA calculation for the nevirapine–Y181C complex using the same procedure. As shown in Table 2, the calculated binding free energy of nevirapine bound to Y181C is −10.29 kcal/mol^{-1} with the new VDW parameters of sulfur. The calculated binding affinity is 1.85 kcal/mol^{-1} lower than that for K103N, which is in better agreement with the experiment than the result obtained using the original VDW parameters of sulfur. Using the new parameters decreases both the electrostatic and van der Waals interactions in Y181C as compared with the results gained from applying the standard Amber force field. The sum of ΔE_{ele} and ΔG_{pol} is 15.59 kcal/mol^{-1}, which is more unfavorable than that (15.07 kcal/mol^{-1}) for the wild type. Therefore, we can conclude that fine tuning of the VDW parameters of sulfur to facilitate interaction with the carbon atom is necessary in the Amber force field.

Mnev-1 First, we also validated the original VDW parameters of sulfur by comparing the interaction energy curve of Mnev-1 with Cys181 calculated at the M06L/6–311++G** level with that obtained from the Amber force field. The energy profile as a function of the distance between N2 of Mnev-1 and the sulfur atom in the side chain of Cys181 is shown in Fig. 8b. Overall, the energies obtained from Amber agree with the QM results very well, so we did not tune the VDW parameters of sulfur when interacting with the nitrogen atom. The binding free energy of Mnev-1 with the wild type obtained from MM/GBSA is −13.20 kcal/mol^{-1}, which is less favorable than that of nevirapine (−14.75 kcal/mol^{-1}). Nevertheless, when we compare the binding free energies of Mnev-1 bound to K103N and Y181C, the corresponding energies are −15.57 and −15.50 kcal/mol^{-1}, respectively, which are more favorable than that of Mnev-1 with the wild type (−13.20 kcal/mol^{-1}) and also more favorable than that of nevirapine bound to the wild-type RT (−14.75 kcal/mol^{-1}). The energies of $\Delta E_{ele}+\Delta G_{pol}$ are 17.52, 17.87, and 17.97 kcal/mol^{-1}, respectively, for the wild type, K103N, and Y181C, which is a

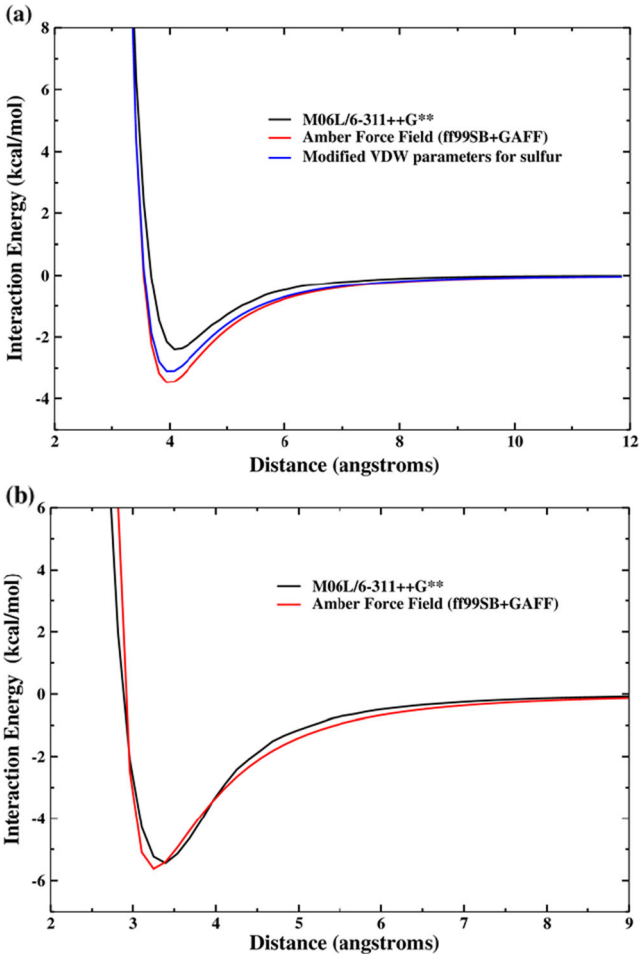

Fig. 8 **a**–**b** Interaction energy profiles between **a** Cys181 and nevirapine; **b** Cys181 and Mnev-1

similar pattern to that seen for nevirapine. However, the van der Waals interactions of Mnev-1 with K103N and Y181C are more favorable than those found for nevirapine. For the wild type, the van der Waals interaction energy of Mnev-1 is −42.04 kcal/mol^{-1}, and this becomes −44.49 and −44.33 kcal/mol^{-1} for K103N and Y181C, respectively. Another important feature that differs from nevirapine is that the entropic penalty becomes smaller upon mutation. As shown in Table 2, $T\Delta S$ for the wild type is −16.27 kcal/mol^{-1}, as compared to −15.73 and −15.76 kcal/mol^{-1} for K103N and Y181C, respectively. Based on our calculations, we predict that Mnev-1 will be more effective at reducing the drug resistance of HIV-1 RT mutants.

Mnev-2 ΔG_{pol} is usually unfavorable for protein–ligand binding. Generally speaking, the more polar groups the inhibitor contains, the greater the value of ΔG_{pol}. If we compare the cases of nevirapine and Mnev-1, which has one more polar hydroxyl group, ΔG_{pol} ranges from 19.77 to 22.10 kcal/mol^{-1} for nevirapine and from 27.79 to 30.60 kcal/mol^{-1} for Mnev-1. Hence, we reduced the number of the polar atoms in Mnev-1 in order to strengthen the overall protein–ligand binding affinity. In the structure of Mnev-2, C16 replaces the N4 atom in Mnev-1 (see Fig. 1), meaning that the range of ΔG_{pol} is reduced to 23.89~27.31 kcal/mol^{-1} for Mnev-2 bound to HIV-1 RT and its mutants. However, the ΔE_{ele} energy is less favorable than that for Mnev-1, and the entropic change is also greater. The total binding free energies are −12.29, −14.76, and −16.32 kcal/mol^{-1} for Mnev-2 bound to the wild type, K103N, and Y181C, respectively—a similar level of performance to that of Mnev-1. The binding free energy of Mnev-2 with the wild type calculated by MM/GBSA is less favorable than that of nevirapine, while Mnev-2 is more favorable than nevirapine binding to the mutated HIV-1 RTs K103N and Y181C. Therefore, we can conclude that Mnev-2 may also be a potential drug candidate for effectively reducing the drug resistance of HIV-1 RT mutants.

Conclusions

In this work, we studied the potencies of two new promising NNRTIs derived from nevirapine (Mnev-1 and Mnev-2) against the wild-type HIV-1 RT and its mutants (K103N and Y181C) using combined molecular docking and MD simulations in explicit water. The MM/GBSA method was used to estimate the binding free energies. In order to make the predicted relative binding affinities of nevirapine bound to the wild-type HIV-1 RT and its mutants agree closely with the experimental values, we also obtained new VDW parameters for the interaction of sulfur with the carbon atom based on ab initio calculations.

Our study demonstrates that each of the new inhibitors (Mnev-1 and Mnev-2) can form a stable hydrogen bond with His235 of the HIV-1 RTs. Moreover, the repulsive interaction with Cys181 in the Y181C–nevirapine complex was also removed from the newly designed inhibitors. The calculated binding free energies for Mnev-1 and Mnev-2 do not decrease upon mutating HIV-1 RT. The binding affinities of the two new inhibitors with K103N and Y181C are more favorable than that of nevirapine bound to the wild type. Overall, our calculations indicate that Mnev-1 and Mnev-2 are potentially potent NNRTI candidates that are active against drug-resistant mutants of HIV-1 RT. Our findings may assist in the design of new NNRTI drugs for the treatment of HIV-1.

Acknowledgments This work was supported by the National Natural Science Foundation of China (grant nos. 10974054, 20933002 and 21303057) and Shanghai PuJiang program (09PJ1404000). X.H. is also supported by the Specialized Research Fund for the Doctoral Program of Higher Education (grant no. 20130076120019) and the Fundamental Research Funds for the Central Universities. We thank the Supercomputer Center of East China Normal University for providing us with computational time.

References

1. Parker WB, White EL, Shaddix SC, Ross LJ, Buckheit RW Jr, Germany JM, Secrist JA, Vince R, Shannon WM (1991) Mechanism of inhibition of human immunodeficiency virus type 1 reverse transcriptase and human DNA polymerases alpha, beta, and gamma by the 5′-triphosphates of carbovir, 3′-azido-3′-deoxythymidine, 2′,3′-dideoxyguanosine and 3′-deoxythymidine. A novel RNA template for the evaluation of antiretroviral drugs. J Biol Chem 266:1754–1762
2. He X, Mei Y, Xiang Y, Zhang DW, Zhang JZH (2005) Quantum computational analysis for drug resistance of HIV-1 reverse transcriptase to nevirapine through point mutations. Proteins 61:423–432
3. Kohlstaedt LA, Wang J, Friedman JM, Rice PA, Steitz TA (1992) Crystal structure at 3.5 Å resolution of HIV-1 reverse transcriptase complexed with an inhibitor. Science 25:1783–1790
4. Wang JM, Morin P, Wang W, Kollman PA (2001) Use of MM-PBSA in reproducing the binding free energies to HIV-1 RT of TIBO derivatives and predicting the binding mode to HIV-1 RT of efavirenz by docking and MM-PBSA. J Am Chem Soc 123:5221–5230
5. Mitsuya H, Yarchoan R, Broder S (1990) Molecular targets for AIDS therapy. Science 249:1533–1544
6. Katz RA, Skalka AM (1994) The retroviral enzymes. Annu Rev Plant Physiol Plant Mol Biol 63:133–173
7. Archer RH, Wisniewski M, Bambara RA, Demeter LM (2001) The Y181C mutant of HIV-1 reverse transcriptase resistant to nonnucleoside reverse transcriptase inhibitors alters the size distribution of RNase H cleavages. Biochemistry 40:4087–4095
8. De Clercq E (1996) Non-nucleoside reverse transcriptase inhibitors (NNRTIs) for the treatment of human immunodeficiency virus type 1 (HIV-1) infections: strategies to overcome drug resistance development. Med Res Rev 16:125–157
9. Kar P, Knecht V (2012) Energetics of mutation-induced changes in potency of lersivirine against HIV-1 reverse transcriptase. J Phys Chem B 116:6269–6278
10. Richman DD, Shih CK, Lowy I, Rose J, Prodanovich P, Goff S, Griffin J (1991) Human immunodeficiency virus type 1 mutants resistant to nonnucleoside inhibitors of reverse transcriptase arise in tissue culture. Proc Natl Acad Sci USA 88:11241–11245
11. Richman DD, Havlir D, Corbeil J, Looney D, Ignacio C, Spector SA, Sullivan J, Cheeseman S, Barringer K, Pauletti D (1994) Nevirapine resistance mutations of human immunodeficiency virus type 1 selected during therapy. J Virol 68:1660–1666
12. Udier-Blagovic M, Tirado-Rives J, Jorgensen WL (2003) Validation of a model for the complex of HIV-1 reverse transcriptase with nonnucleoside inhibitor TMC125. J Am Chem Soc 125:6016–6017
13. Nikolenko GN, Kotelkin AT, Oreshkova SF, Ilyichev AA (2011) Mechanisms of HIV-1 drug resistance to nucleoside and nonnucleoside reverse transcriptase inhibitors. Mol Biol 45:93–109
14. De Clercq E (2002) New developments in anti-HIV chemotherapy. Biochim Biophys Acta Mol Basis Dis 1587:258–275
15. Sardana VV, Emini EA, Gotlib L, Graham DJ, Lineberger DW, Long WJ, Schlabach AJ, Wolfgang JA, Condra JH (1992) Functional analysis of HIV-1 reverse transcriptase amino acids involved in resistance to multiple nonnucleoside inhibitors. J Biol Chem 267: 17526–17530
16. Richman DD (1993) Resistance of clinical isolates of human immunodeficiency virus to antiretroviral agents. Antimicrob Agents Chemother 37:1207–1213
17. Schinazi RF, Larder BA, Mellors JW (2000) Mutations in retroviral genes associated with drug resistance: 2000–2001 update. Int Antivir News 6:65–91
18. Young SD, Britcher SF, Tran LO, Payne LS, Lumma WC, Lyle TA, Huff JR, Anderson PS, Olsen DB, Carroll SS (1995) L-743, 726 (DMP-266): a novel, highly potent nonnucleoside inhibitor of the human immunodeficiency virus type 1 reverse transcriptase. Antimicrob Agents Chemother 39:2602–2605
19. Zhan P, Liu XY, Li ZY, Pannecouque C, De Clercq E (2009) Design strategies of novel NNRTIs to overcome drug resistance. Curr Med Chem 16:3903–3917
20. Song Y, Zhan P, Kang DW, Li X, Tian Y, Li ZY, Chen XW, Chen WM, Pannecouque C, De Clercq E, Liu XY (2013) Discovery of novel pyridazinylthioacetamides as potent HIV-1 NNRTIs using a structure-based bioisosterism approach. Med Chem Commun 4:810–816
21. Parrish J, Tong L, Wang M, Chen XW, Lansdon EB, Cannizzaro C, Zheng XB, Desai MC, Xu LH (2013) Synthesis and biological evaluation of phosphonate analogues of nevirapine. Bioorg Med Chem Lett 23:1493–1497
22. Rizzo RC, Tirado-Rives J, Jorgensen WL (2001) Estimation of binding affinities for HEPT and nevirapine analogues with HTV-1 reverse transcriptase via Monte Carlo simulations. J Med Chem 44: 145–154
23. Rizzo RC, Udier-Blagovic M, Wang DP, Watkins EK, Smith MBK, Smith RH, Tirado-Rives J, Jorgensen WL (2002) Prediction of activity for nonnucleoside inhibitors with HIV-1 reverse transcriptase based on Monte Carlo simulations. J Med Chem 45:2970–2987
24. Wang DP, Rizzo RC, Tirado-Rives J, Jorgensen WL (2001) Antiviral drug design: computational analyses of the effects of the L100I mutation for HIV-RT on the binding of NNRTIs. Bioorg Med Chem Lett 11:2799–2802
25. Zhang DW, Zhang JZH (2003) Molecular fractionation with conjugate caps for full quantum mechanical calculation of protein–molecule interaction energy. J Chem Phys 119:3599–3605
26. Zhang DW, Chen XH, Zhang JZH (2003) Molecular caps for full quantum mechanical computation of peptide–water interaction energy. J Comput Chem 24:1846–1852
27. Chen XH, Zhang DW, Zhang JZH (2004) Fractionation of peptide with disulfide bond for quantum mechanical calculation of interaction energy with molecules. J Chem Phys 120:839–844
28. Zhang DW, Zhang JZH (2004) Full ab initio computation of protein–water interaction energies. J Theor Comput Chem 3:43–49
29. Zhang DW, Xiang Y, Zhang JZH (2003) New advance in computational chemistry: full quantum mechanical ab initio computation of streptavidin–biotin interaction energy. J Phys Chem B 107: 12039–12041
30. Zhang DW, Xiang Y, Gao AM, Zhang JZH (2004) Quantum mechanical map for protein–ligand binding with application to beta-trypsin/benzamidine complex. J Chem Phys 120:1145–1148
31. Mei Y, He X, Xiang Y, Zhang DW, Zhang JZH (2005) Quantum study of mutational effect in binding of efavirenz to HIV-1 RT. Proteins 59:489–495
32. Mei Y, He X, Ji CG, Zhang DW, John ZHZ (2012) A fragmentation approach to quantum calculation of large molecular systems. Prog Chem 24:1058–1064
33. Wang XW, Liu JF, Zhang JZH, He X (2013) Electrostatically embedded generalized molecular fractionation with conjugate caps method for full quantum mechanical calculation of protein energy. J Phys Chem A 117:7149–7161
34. He X, Zhang JZH (2006) The generalized molecular fractionation with conjugate caps/molecular mechanics method for direct calculation of protein energy. J Chem Phys 124:184703
35. He X, Zhang JZH (2005) A new method for direct calculation of total energy of protein. J Chem Phys 122:031103
36. He X, Merz KM (2010) Divide and conquer Hartree–Fock calculations on proteins. J Chem Theory Comput 6:405–411
37. Wang JM, Hou TJ, Xu XJ (2006) Recent advances in free energy calculations with a combination of molecular mechanics and continuum models. Curr Comput Aided Drug Des 2:287–306
38. Kollman PA, Massova I, Reyes C, Kuhn B, Huo SH, Chong L, Lee M, Lee T, Duan Y, Wang W, Donini O, Cieplak P, Srinivasan J, Case

DA, Cheatham TE (2000) Calculating structures and free energies of complex molecules: combining molecular mechanics and continuum models. Acc Chem Res 33:889–897
39. Liu JF, He X, Zhang JZH (2013) Improving the scoring of protein–ligand binding affinity by including the effects of structural water and electronic polarization. J Chem Inf Model 53:1306–1314
40. Weis A, Katebzadeh K, Soderhjelm P, Nilsson I, Ryde U (2006) Ligand affinities predicted with the MM/PBSA method: dependence on the simulation method and the force field. J Med Chem 49:6596–6606
41. Wang W, Donini O, Reyes CM, Kollman PA (2001) Biomolecular simulations: recent developments in force fields, simulations of enzyme catalysis, protein–ligand, protein–protein, and protein–nucleic acid noncovalent interactions. Annu Rev Biophys Biomol Struct 30: 211–243
42. Onufriev A, Bashford D, Case DA (2000) Modification of the generalized Born model suitable for macromolecules. J Phys Chem B 104:3712–3720
43. Onufriev A, Bashford D, Case DA (2004) Exploring protein native states and large-scale conformational changes with a modified generalized Born model. Proteins 55:383–394
44. Hou TJ, Wang JM, Li YY, Wang W (2011) Assessing the performance of the MM/PBSA and MM/GBSA methods. 1. The accuracy of binding free energy calculations based on molecular dynamics simulations. J Chem Inf Model 51:69–82
45. Rastelli G, Del Rio A, Degliesposti G, Sgobba M (2010) Fast and accurate predictions of binding free energies using MM-PBSA and MM-GBSA. J Comput Chem 31:797–810
46. Morris GM, Goodsell DS, Halliday RS, Huey R, Hart WE, Belew RK, Olson AJ (1998) Automated docking using a Lamarckian genetic algorithm and an empirical binding free energy function. J Comput Chem 19:1639–1662
47. Case DA, Cheatham TE, Darden T, Gohlke H, Luo R, Merz KM, Onufriev A, Simmerling C, Wang B, Woods RJ (2005) The Amber biomolecular simulation programs. J Comput Chem 26:1668–1688
48. Hornak V, Abel R, Okur A, Strockbine B, Roitberg A, Simmerling C (2006) Comparison of multiple Amber force fields and development of improved protein backbone parameters. Proteins 65:712–725
49. Wang JM, Wang W, Kollman PA, Case DA (2006) Automatic atom type and bond type perception in molecular mechanical calculations. J Mol Graph Model 25:247–260
50. Wang JM, Wolf RM, Caldwell JW, Kollman PA, Case DA (2004) Development and testing of a general Amber force field. J Comput Chem 25:1157–1174
51. Bayly CI, Cieplak P, Cornell W, Kollman PA (1993) A well-behaved electrostatic potential based method using charge restraints for deriving atomic charges: the RESP model. J Phys Chem 97:10269–10280
52. Cornell WD, Cieplak P, Bayly CI, Kollmann PA (1993) Application of RESP charges to calculate conformational energies, hydrogen bond energies, and free energies of solvation. J Am Chem Soc 115: 9620–9631
53. Frisch MJ, Trucks GW, Schlegel HB, Scuseria GE, Robb MA, Cheeseman JR, Scalmani G, Barone V, Mennucci B, Petersson GA, Nakatsuji H, Caricato M, Li X, Hratchian HP, Izmaylov AF, Bloino J, Zheng G, Sonnenberg JL, Hada M, Ehara M, Toyota K, Fukuda R, Hasegawa J, Ishida M, Nakajima T, Honda Y, Kitao O, Nakai H, Vreven T, Montgomery JA Jr, Peralta JE, Ogliaro F, Bearpark M, Heyd JJ, Brothers E, Kudin KN, Staroverov VN, Keith T, Kobayashi R, Normand J, Raghavachari K, Rendell A, Burant JC, Iyengar SS, Tomasi J, Cossi M, Rega N, Millam JM, Klene M, Knox JE, Cross JB, Bakken V, Adamo C, Jaramillo J, Gomperts R, Stratmann RE, Yazyev O, Austin AJ, Cammi R, Pomelli C, Ochterski JW, Martin RL, Morokuma K, Zakrzewski VG, Voth GA, Salvador P, Dannenberg JJ, Dapprich S, Daniels AD, Farkas O, Foresman JB, Ortiz JV, Cioslowski J, Fox DJ (2010) Gaussian 09, revision B.01. Gaussian, Inc., Wallingford
54. Darden T, York D, Pedersen L (1993) Particle mesh Ewald: an N-log(N) method for Ewald sums in large systems. J Chem Phys 98: 10089–10093
55. Ryckaert JP, Ciccotti G, Berendsen HJC (1977) Numerical integration of the cartesian equations of motion of a system with constraints: molecular dynamics of *n*-alkanes. J Comput Phys 23:327–341
56. Pastor RW, Brooks BR, Szabo A (1988) An analysis of the accuracy of Langevin and molecular dynamics algorithms. Mol Phys 65:1409–1419
57. Weiser J, Shenkin PS, Still WC (1999) Approximate atomic surfaces from linear combinations of pairwise overlaps (LCPO). J Comput Chem 20:217–230
58. Genheden S, Kuhn O, Mikulskis P, Hoffmann D, Ryde U (2012) The normal-mode entropy in the MM/GBSA method: effect of system truncation, buffer region, and dielectric constant. J Chem Inf Model 52:2079–2088
59. Schaefer W, Friebe WG, Leinert H, Mertens A, Poll T, Saal WVD, Zilch H, Nuber B, Ziegler ML (1993) Non-nucleoside inhibitors of HIV-1 reverse transcriptase: molecular modeling and X-ray structure investigations. J Med Chem 36:726–732
60. Cornell WD, Cieplak P, Bayly CI, Gould IR, Merz KM Jr, Ferguson DM, Spellmeyer DC, Fox T, Caldwell JW, Kollman PA (1995) A second generation force field for the simulation of proteins, nucleic acids, and organic molecules. J Am Chem Soc 117:5179–5197
61. Wang JM, Kang XS, Kuntz ID, Kollman PA (2005) Hierarchical database screenings for HIV-1 reverse transcriptase using a pharmacophore model, rigid docking, solvation docking, and MM-PB/SA. J Med Chem 48:2432–2444